Bioorganic & Medicinal Chemistry 16 (2008) 7759–7769

Contents lists available at ScienceDirect

Bioorganic & Medicinal Chemistry

journal homepage: www.elsevier.com/locate/bmc

New tacrine-dihydropyridine hybrids that inhibit acetylcholinesterase, calcium entry, and exhibit neuroprotection properties

Rafael León [a,b,*], Cristóbal de los Ríos [a,b], José Marco-Contelles [a,*], Oscar Huertas [d], Xavier Barril [e], F. Javier Luque [d,*], Manuela G. López [b], Antonio G. García [b,c], Mercedes Villarroya [b,*]

[a] Laboratorio de Radicales Libres (IQOG, CSIC), C/Juan de la Cierva 3, 28006 Madrid, Spain
[b] Instituto Teófilo Hernando, Departamento de Farmacología y Terapéutica, Facultad de Medicina, Universidad Autónoma de Madrid, C/Arzobispo Morcillo 4, 28029 Madrid, Spain
[c] Servicio de Farmacología Clínica, Hospital Universitario de la Princesa, C/Diego de León 62, 28006 Madrid, Spain
[d] Departament de Fisicoquímica and Institut de Biomedicina (IBUB), Facultat de Farmàcia, Universitat de Barcelona, Avda. Diagonal 643, Barcelona, Spain
[e] Institució Catalana de Recerca i Estudis Avançats (ICREA), Departament de Fisicoquímica and Institut de Biomedicina, Facultat de Farmàcia, Universitat de Barcelona, Avda. Diagonal 643, Barcelona, Spain

ARTICLE INFO

Article history:
Received 6 February 2008
Revised 24 June 2008
Accepted 2 July 2008
Available online 8 July 2008

Keywords:
Tacrine-dihydropyridine hybrids
AChE
BuChE
Kinetic analysis
Inhibition mechanism
Voltage-dependent calcium channels
Neuroprotection
Molecular modeling

ABSTRACT

In this communication, we describe the synthesis and biological evaluation of tacripyrimedones **1**–**5**, a series of new tacrine-1,4-dihydropyridine hybrids bearing the general structure of 11-amino-12-aryl-3,3-dimethyl-3,4,5,7,8,9,10,12-octahydrodibenzo[*b*,*g*][1,8]naphthyridine-1(2*H*)-one. These multifunctional compounds are moderately potent and selective AChEIs, with no activity toward BuChE. Kinetic analysis and molecular modeling studies point out that the new compounds preferentially bind the peripheral anionic site of AChE. In addition, compounds **1**–**5** show an excellent neuroprotective profile, and a moderate blocking effect of L-type voltage-dependent calcium channels due to the mitigation of $[Ca^{2+}]$ elevation elicited by K^+ depolarization. Therefore, they represent a new family of molecules with potential therapeutic application for the treatment of Alzheimer's disease.

1. Introduction

Alzheimer's disease (AD) is an age-related neurodegenerative disease characterized by progressive memory loss and other cognitive impairments. Although the etiology of AD is not well known, there are diverse factors such as amyloid-β (Aβ) deposits, τ-protein aggregation, oxidative stress, or low levels of acetylcholine (ACh) that are thought to play significant roles in the disease.[1] The cholinergic theory of AD suggests that the selective loss of cholinergic neurons in AD results in a deficit of ACh in specific regions of the brain that mediate learning and memory functions.[2] The primary approach for treating AD has, therefore, aimed at increasing the ACh levels in the brain by using acetylcholinesterase inhibitors (AChEIs) such as donepezil, galantamine, or rivastigmine.[3] On the other hand, Ca^{2+} overload seems to be the main factor initiating the processes leading to cell death. Several lines of evidence show that Ca^{2+} dysfunction, involved in the pathogenesis of AD,[4] augments Aβ formation,[5a] and τ hyperphosphorylation.[5b] Ca^{2+} entry through the L-subtype of high-voltage activated Ca^{2+} channels ($Ca_v1.1$–1.4) causes both Ca^{2+} overload and mitochondrial disruption, which activate the apoptotic cascade and cell death.[6] Hence, blocking the entrance of Ca^{2+} through calcium channels could be a good strategy to prevent cell death.

The current multi-target approach in drug design[7] for the treatment of AD includes novel tacrine–melatonin hybrids,[8a] dual inhibitors of AChE and monoamine oxidase (MAO),[8b] dual AChEI and serotonin transporters inhibitors,[8c] potent AChEIs with antioxidant and neuroprotective properties,[8d] or gallamine–tacrine hybrids designed to bind the cholinergic and M_2 muscarinic receptors.[8e]

Since 1,4-dihydropyridines (DHPs) are compounds that selectively block L-type Ca^{2+} channels, we considered the synthesis and the pharmacological study of new multipotent hybrid compounds, based on an AChEI and a DHP, such as tacrine and nimodipine (Chart 1).[9] Besides inhibition of AChE and blockade of voltage-dependent calcium channels (VDCC), we were also interested in compounds targeted to prevent oxidative stress. Recent research has demonstrated that oxidative damage is an event that precedes

* Corresponding authors. Tel.: +34 91 5622900; fax: +34 91 5644853.
E-mail addresses: iqoc21@iqog.csic.es (J. Marco-Contelles), fjluque@ub.edu (F. Javier Luque).

0968-0896/$ - see front matter © 2008 Elsevier Ltd. All rights reserved.
doi:10.1016/j.bmc.2008.07.005

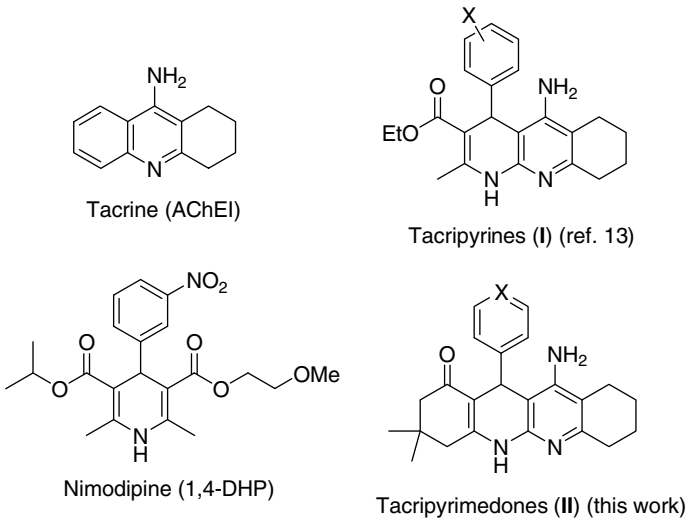

Chart 1.

the appearance of other pathological hallmarks of AD.[10] Thus, drugs that scavenge reactive oxygen species (ROS) may have a particular therapeutic efficacy.[11,12]

Based on this strategy, we have recently reported preliminary studies on the synthesis and biological activity of ethyl esters of 5-amino-4-aryl-1,4,6,7,8,9-hexahydro-2-methyl-benzo[*b*][1,8]naphthyridine-3-carboxylic acid (**I**) (Chart 1) that we have named as tacripyrines, as the first examples of tacrine-DHP hybrids described in the literature.[13] Prompted by the interesting biological profile of these compounds (very selective and potent AChEIs, excellent neuroprotective profile and moderate Ca^{2+} channel blockade effects), we have now prepared new analogs of the general structure **II** (Chart 1), for which we propose the short name of tacripyrimedones, where we have incorporated a functionalized cyclohexane ring annulated onto the DHP-ring present in type **I** compounds, in order to start a general structure–activity relationship (SAR) analysis targeted to improve the biological activities found in the lead-type compounds **I**.[13]

Accordingly, in this work we report the synthesis and biological evaluation, including AChE/BuChE (butyrylcholinesterase) inhibition, kinetic analysis, and molecular modeling of the AChE inhibition, blockade of cytosolic Ca^{2+} elevation, and the neuroprotective activity for the novel tacrine-DHP hybrids tacripyrimedones **1–5** (Scheme 1).

2. Results and discussion

2.1. Synthesis of 11-amino-12-aryl-3,3-dimethyl-3,4,5,7,8,9,10,12-octahydrodibenzo[*b*,*g*][1,8]naphthyridine-1(2*H*)-ones (1–5)

The synthesis of tacripyrimedones **1–5** was easily achieved, in excellent yields, using the Friedländer reaction[14] between 2-amino-4-aryl-7,7-dimethyl-5-oxo-1,4,5,6,7,8-hexahydroquinoline-3-carbonitriles (**6–10**)[15] and cyclohexanone, under standard conditions (Scheme 1).[16] Precursors **6–10**, readily available compounds in multigram quantities, are prepared by refluxing equimolar amounts of the corresponding arylidenemalononitrile, dimedone, and an excess of ammonium acetate in acetic acid as solvent.[15]

Compounds **1–5** are racemic octahydrobenzo[*b*,*g*][1,8]naphthyridines substituted at C12 with an aromatic ring, incorporating different types of substituents at C4′ (**1–4**) or a 4′-pyridyl ring (**5**). These molecules have been conveniently characterized by their spectroscopic and analytical data. The ^1H and ^{13}C NMR data (see Section 4) are in good agreement with the values found for related

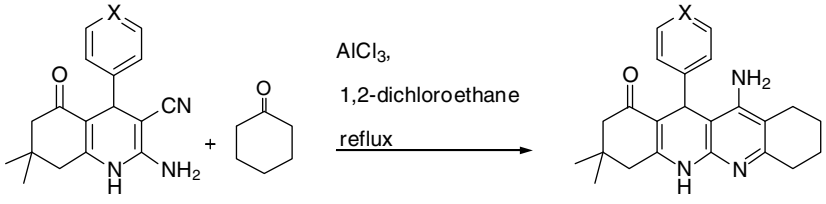

6 X= C-H
7 X= C-F
8 X= C-Me
9 X= C-OMe
10 X= N

1 (97%)
2 (90%)
3 (96%)
4 (83%)
5 (88%)

Scheme 1.

compounds,[13,15] and the assignments are based on standard NMR experiments (^{1}H–^{1}H COSY, HMQC, and HMBC).

2.2. Pharmacology

2.2.1. Studies of AChE/BuChE inhibition

According to standard methodology[17,18] (see Section 4), tacripyrimedones **1–5** have been evaluated as possible inhibitors of AChE from both *Electrophorus electricus* (electric eel) and human erythrocytes, and of BuChE from human serum. The IC_{50} values corresponding to compounds **1–5**, and those observed for related AChEIs **11–14** as well as for tacrine, which is used as reference compound,[13] are shown in Table 1.

Regardless of the AChE origin (*Ee* or human erythrocytes), compounds **1–5** were submicromolar AChE inhibitors with similar potency for the inhibition of both AChEs, as noted by IC_{50} values ranging from 0.22 to 0.60 μM (for *Ee*AChE) and from 0.37 to 2.80 μM (for hAChE), which were also similar to the IC_{50} value determined for tacrine (0.18 and 0.15 μM, respectively). Compounds **1–5** were much more selective than tacrine versus AChE; none of the new tacrine-DHP hybrids inhibited this enzyme (the hBuChE/hAChE ratio varies from >36 to >270; Table 1).

Considering the type of substituent at C4′ in the aromatic ring, the substitution of the hydrogen in the parent compound (**1**) by an electron-withdrawing group (4′-F, 4′-pyridyl) reduced the *Ee*AChE inhibition by a factor of 1.6–1.8, while the incorporation of an electron-donating substituent (Me and OMe) led to a 1.4-fold increase in the AChE inhibition. Similar trends were found for the dependence of the hAChE inhibition on the substituent at the aromatic ring. Finally, all the new derivatives **1–5** were less active than compounds **11–14**[13] (Table 1) on AChE by a factor ranging from 2.5 (3.5) for the pair of compounds **3** and **13** to 10 (8.2) for the pair **2** and **12** in *Ee*AChE (hAChE).

We have reported that compounds **17** and **18**[20] (Chart 2) showed slightly lower (from two to fourfold less) AChE inhibitory potencies (Table 2). Compounds **19–22**, which did not show BuChE activity,[15b] had significantly higher AChE IC_{50} values than those relative to **1–5**, which were nearly 100-fold more potent (Table 2), even though the only structural difference was the replacement of the oxygen atom at C4 in **19–22** by the N–H unit in **1–5** (Chart 2). These results agree with previous works from our laboratory[13] where the insertion of the –NH– unit in the heterocyclic ring enhanced the AChE inhibitory activity for type **I** compounds (about 100-fold more active than compounds **15–18**). SAR study of these derivatives and analogs also pointed out the importance of the NH unit present in the dihydropyridine ring.

Previous studies from our laboratories concluded that compounds **15** and **16** proved to be non-competitive inhibitors of AChE (Chart 2),[19] which suggest interaction at the PAS of AChE. This assumption was supported by molecular modeling studies, which revealed a large structural distortion upon forcing binding of **16** at the catalytic site of AChE.[19a] Moreover, since compounds **1–5** are bulkier than compound **16** due to the tetracyclic system, access to the AChE catalytic site through the narrow gorge would be more difficult, thus supporting the feasibility of the interaction with the PAS of the enzyme. On the other hand, even though AChE and BuChE share most of the structural and physicochemical properties,[21a] BuChE does not possess a peripheral site. This structural difference would thus explain why compounds **1–5** are strong inhibitors of AChE, but have no relevant activity on BuChE.

2.2.2. Mechanism of AChE inhibition

One of the hallmarks of AD lies in the formation of senile plaques by accumulation of the Aβ peptide. Different studies have proven that AChE binds to Aβ inducing the formation of fibrils[21b] and that the PAS of the enzyme is involved in catalyzing the aggregation.[22] Ligands like propidium iodide that bind to the PAS are known to block Aβ aggregation.[22] Consequently, inhibitors which are able to bind the PAS can be of utmost interest for their potential use for the treatment of AD. AChE possesses an active site at which substrates like ACh and acetylthiocholine (ATCh) are hydrolyzed, and a PAS, which is spatially distinct from the active center and

Table 1
Inhibition of AChE and BuChE (IC_{50}) by compounds **1–5**[a] and **11–14**[13]

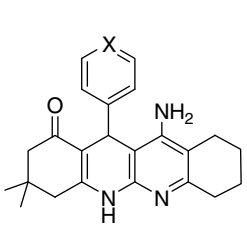

1-5

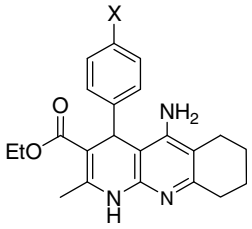

11-14

	X	IC_{50} (μM) *Ee*AChE[b]	IC_{50} (μM) hAChE	IC_{50} (μM) hBuChE[c]	Selectivity[d]
Tacrine[13]	—	0.18 ± 0.01	0.15 ± 0.01	0.036	0.24
1	C-H	0.32 ± 0.02	0.71 ± 0.03	>100	>141
2	C-F	0.54 ± 0.04	1.6 ± 0.2	>100	>63
3	C-Me	0.23 ± 0.01	0.67 ± 0.07	>100	>149
4	C-OMe	0.22 ± 0.02	0.37 ± 0.01	>100	>270
5	N	0.6 ± 0.3	2.8 ± 0.1	>100	>36
11[13]	H	0.080 ± 0.001	0.12 ± 0.21	>100	>819
12[13]	F	0.052 ± 0.009	0.19 ± 0.03	>100	>518
13[13]	Me	0.091 ± 0.004	0.17 ± 0.01	>100	>592
14[13]	OMe	0.045 ± 0.005	0.11 ± 0.01	>100	>952

[a] IC_{50} values are means ± SEM of at least three independent measurements.
[b] *Ee*, *Electrophorus electricus*.
[c] h, human.
[d] hBuChE/hAChE.

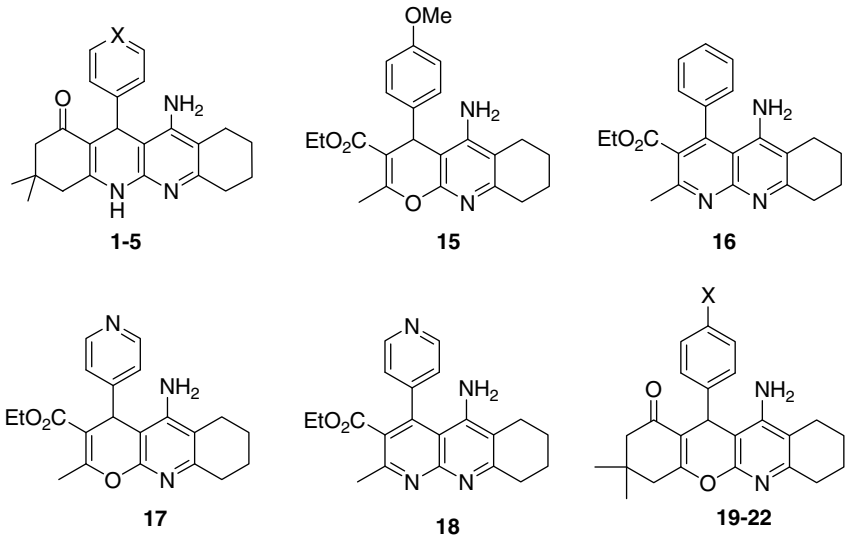

Chart 2.

Table 2
Inhibition of AChE by compounds **1**–**5** and **15**–**22**[a]

	X	IC_{50} *Ee*AChE (μM)
Tacrine[13]	—	0.18 ± 0.01
1	C-H	0.32 ± 0.02
2	C-F	0.54 ± 0.04
3	C-Me	0.23 ± 0.01
4	C-OMe	0.22 ± 0.02
5	X = N	0.60 ± 0.30
15[19]	—	0.87 ± 0.20
16[19]	—	0.82 ± 0.40
17[20]	—	3.00 ± 0.30
18[20]	—	1.40 ± 0.40
19[15c]	H	49.0 ± 1.00
20[15c]	F	70.0 ± 5.00
21[15c]	Me	52.0 ± 2.00
22[15c]	OMe	4.10 ± 3.00

[a] IC_{50} values are means ± SEM of at least three independent measurements.

where selective inhibitors can bind with high affinity and specificity.[23] Hydrolysis of ACh proceeds through the formation of an acyl-enzyme intermediate, and inhibitors that bind the PAS can also affect steady-state kinetics.[24]

Based on the preceding considerations and on the hypothesis that the rather wide shape of molecules such as **1**–**5** might impair the entrance into the AChE gorge and favor the binding at the PAS, we studied the steady-state kinetics of compounds **1–5** as well as that of tacrine and propidium. The graphical analysis of the steady-state inhibition data can give information about the binding mode of the selected compounds, and allow the measurement of their K_i, as well.

The kinetic characterization of these AChE inhibitors was carried out as follows. Reactions were measured in the presence of different concentrations of substrate and data were analyzed according to the Linewever–Burk method (Fig. 1). Five different concentrations of each inhibitor were used. Values of K_i were calculated from the slope of a secondary plot (see Section 4 and Table 3).

The K_i value found for tacrine agrees with the data reported in the literature,[25] and the reciprocal plots describing the AChE inhibition (Fig. 1A) show both increasing slopes and increasing intercepts with higher inhibition concentration, a pattern that indicates mixed inhibition. In the reciprocal plots for compound **4** and propidium (Fig. 1B and C, respectively), lines crossing the *x* axis in the same point reveal unchanged K_m and decreased V_{max} at increasing inhibitor concentrations. This is a typical trend for non-competitive inhibition, and indicates that these compounds bind to a site different to the catalytic one.[26] Since propidium has been described as a selective ligand for the AChE PAS,[23] the same behavior is therefore expected for compound **4**.

The hypothesis of the binding at the AChE PAS for tacripyrimedones **1**–**5** is also consistent with their BuChE/AChE selectivity (Table 1), since binding at the PAS is mediated by the residue Trp279 (*Ee*AChE) present at the entrance of the gorge in AChE, but absent in BuChE.

2.2.3. Molecular modeling

The AChE binding mode of tacripyrimedones **1**–**5** (Scheme 1) was explored by means of docking studies performed for **4** in hAChE using the rDock program (see Section 4). To verify the reliability of the docking protocol, docking was also extended to tacrine and propidium taking advantage of the known X-ray crystallographic binding mode of these compounds at the catalytic and peripheral sites, respectively, of AChE. The docking results confirmed the capability of the method to reproduce the experimental binding mode (see Figs. 2 and 3), thus giving confidence to the binding mode predicted for **4**.

Attempts to dock **4** in the catalytic site of hAChE were unsuccessful, as expected from our previous molecular dynamics studies performed for **15** and **16**[19a] (Chart 2), which pointed out that the catalytic site of AChE is not flexible enough to easily accommodate those compounds. In contrast, it was successfully docked in the PAS, which is in agreement with the non-competitive inhibition mechanism exhibited by **4**. According to the putative binding mode of the *R*-enantiomer of **4** (see Fig. 4), the inhibitor is well stacked against the indole ring of Trp286 (hAChE, with a distance from the central aminopyridine unit of **4** to the midpoint of the indole ring of Trp286 of ~3.6 Å), while forming hydrogen-bonds with several residues. Thus, the NH group of the 1,8-naphthyridine unit is hydrogen-bonded to the hydroxyl group of Tyr72, which in turn is hydrogen-bonded to the carboxylate group of Asp74 (the latter group might also form hydrogen-bond interactions with Tyr341 and Thr83). The oxygen atom of the carbonyl group is correctly positioned to hydrogen-bond to the imidazole ring of His287, thus mimicking a similar interaction found between one of the NH_2

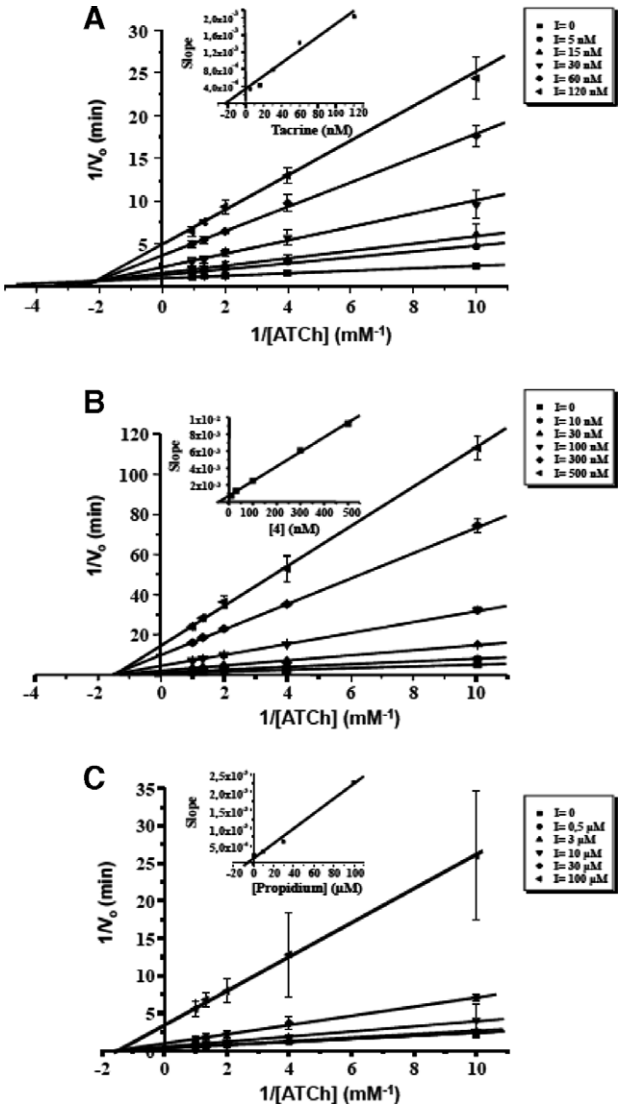

Figure. 1. Double reciprocal plots of the reaction velocity versus acetyltiocholine (ATCh) concentration in the presence and absence of inhibitor. The study was performed in 0.1 M PBS solution, pH 8 and five different concentrations of substrate. Concentrations of tacrine, compound **4**, and propidium were as follows. Tacrine: Control (■) [I] = 0, (●) [I] = 5 nM, (▲) [I] = 15 nM, (▼) [I] = 30 nM, (♦) [I] = 60 nM, (?) [I] = 500 nM. Compound **4**: Control (■) [I] = 0, (●) [I] = 5 nM, (▲) [I] = 15 nM, (▼) [I] = 30 nM, (♦) [I] = 60 nM, (?) [I] = 120 nM. Propidium: Control (■) [I] = 0, (●) [I] = 0,5 nM, (▲) [I] = 1 μM, (▼) [I] = 10 μM, (♦) [I] = 30 μM, (?) [I] = 100 μM. (A) Lineweaver–Burk study of tacrine. Insert: slope (■) of the double reciprocal plots versus [tacrine]. (B) Lineweaver–Burk study of compound **4**. Insert: slope (■) of the double reciprocal plots versus [**4**]. (C) Lineweaver–Burk study of propidium. Insert: slope (■) of the double reciprocal plots versus [propidium]. Data are expressed as mean ± SEM of at least four experiments.

groups in propidium with His287 (PDB entry 1N5R). Finally, the amino group is properly oriented toward the hydroxyl and carbonyl groups of Ser293, even though those interactions should be

Table 3
IC_{50} for inhibition of AChE, K_i's and type of inhibition for tacrine, propidium, and compounds **1**–**5** with *Ee*AChE

	IC_{50} AChE (μM)	K_i ± SE (nM)	Type of inhibition
Tacrine	0.18	20.2 ± 0.12	Mixed
1	0.32	61.3 ± 3.21	Non-competitive
2	0.54	106.0 ± 4.67	Non-competitive
3	0.23	38.9 ± 1.85	Non-competitive
4	0.22	41.9 ± 2.52	Non-competitive
5	0.60	157.0 ± 4.76	Non-competitive
Propidium	11.0	6800 ± 60	Non-competitive

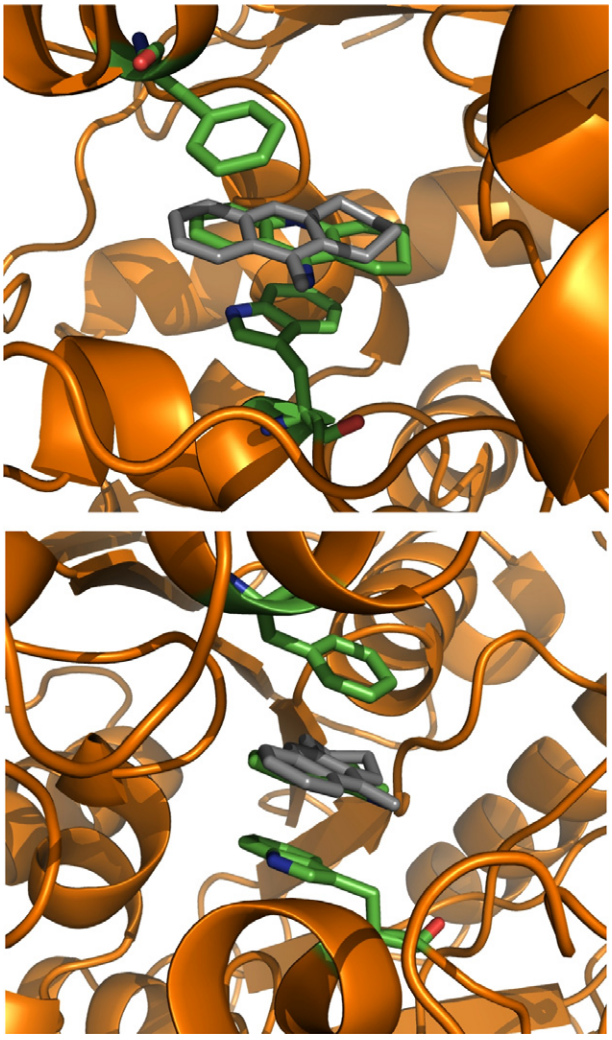

Figure. 2. Two views of the predicted binding mode of tacrine at the catalytic site of the AChE, taking advantage of the X-ray crystallographic structures of the *Torpedo californica* AChE complex (PDB entry 1ACJ). Docked and X-ray structures of the ligand are colored by atom and in gray, respectively. For the sake of clarity, hydrogen atoms are omitted.

assisted by a water molecule as the distance between the interacting groups of inhibitor and Ser293 amounts to ~6.4 Å. Finally, the 4′-methoxybenzene unit is pointing toward the solvent, adopting a similar arrangement as the aliphatic chain containing the quaternary ammonium group in propidium, thus avoiding steric clashes with residues at the PAS.

It is worth-noting that these features allow us to explain the 100-fold increase in the inhibitory potency observed when comparing compounds **1**–**4** to **19**–**22** (see above and Table 2); this difference can be ascribed to the loss of the hydrogen-bond interaction formed between the inhibitor and Tyr72 upon replacement of the NH moiety by O. Furthermore, since a similar change in the inhibitory potency is observed for compounds **11**–**14** relative to **15**–**18**, it can be speculated that tacripyrines **I** bind to the PAS of AChE mimicking the binding mode of **4**. This binding mode would also explain the relative insensitivity of the inhibitory potency of compounds **1**–**4** to the presence of the substituent in position 4′ or to the replacement of the benzene ring by a pyridine in **5** (see Table 1). Finally, the slightly lower potency of compounds **1**–**4** relative to **11**–**14** likely reflects a decrease in the flexibility of the carbonyl group to interact with

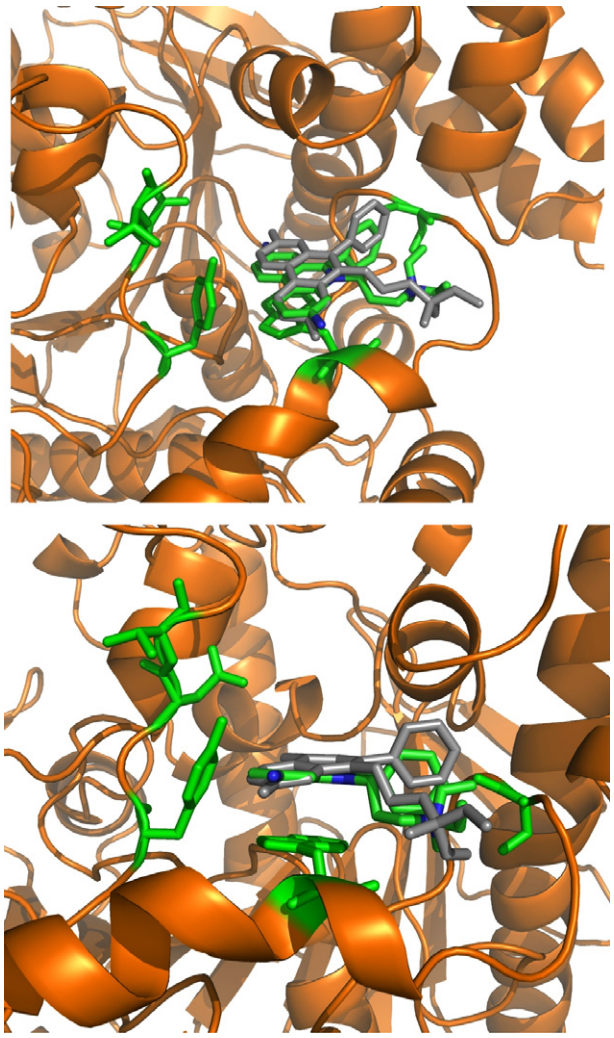

Figure. 3. Two views of the predicted binding mode of propidium at the peripheral site of the AChE, taking advantage of the X-ray crystallographic structures of the mouse AChE complex (PDB entry 1N5R). Docked and X-ray structures are colored by atom and in gray, respectively. For the sake of clarity, hydrogen atoms are omitted.

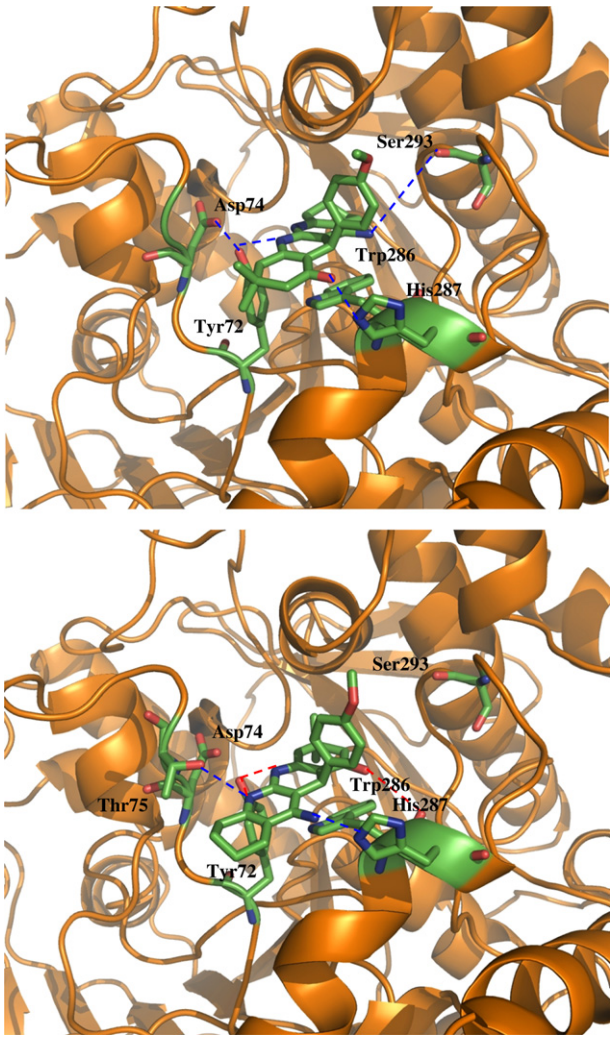

Figure. 4. Representation of the putative binding modes of *R* (top) and *S* (bottom) enantiomers of compound **4** (colored by atom) in the PAS of hAChE (shown by ribbon). Selected residues of the protein are also displayed (Trp286 (hAChE), Tyr72, Asp74, His287, and Ser293; Thr75 is also shown in the bottom plot). Favorable hydrogen-bond interactions are shown by blue lines, and unfavorable contacts are shown by red lines (see text for details). For the sake of clarity, hydrogen atoms are omitted.

His287. On the other hand, the lack of a tryptophan residue mimicking Trp286 (hAChE) in the peripheral site of hBuChE (replaced by Ala277), as well as the replacement of Tyr72 in hAChE by Asn68 in hBuChE, could also explain the large AChE/BuChE selectivity of these compounds.

Finally, binding of the *S*-enantiomer of **4** (see Fig. 4) appears to be less favorable. Thus, even though the inhibitor is stacked against Trp286 (hAChE) and the 4′-methoxybenzene unit has a similar orientation in the binding modes of *R*- and *S*-enantiomers, the inhibitor is not as buried in the PAS as the *R*-enantiomer. Moreover, the alternative hydrogen-bond interactions formed between the 1,8-naphthyridine NH and NH_2 groups with Thr75 and His287 are counterbalanced by unfavorable contacts, such as those due to the carbonyl and pyridine nitrogen groups of *S*-**4**, which are pointing toward the Trp286 (hAChE) carbonyl (O···O distance of ~3.9 Å) and Tyr72 oxygen (N···O distance of ~2.9 Å) groups, respectively.

Overall, these results suggest that the AChE inhibitory potency of tacripyrimedones **1**–**5** should be ascribed to the *R*-enantiomer, whose binding mode in the PAS provides a basis to explain the non-competitive inhibition of these compounds and the main conclusions of the SAR study.

2.3. Effects of new compounds on the changes of $[Ca^{2+}]_c$ evoked by K^+

Since our therapeutic strategy pursues the design of new multipotent drugs for the treatment of Alzheimer's disease, we have investigated the effect of compounds **1**–**5** on the elevations of $[Ca^{2+}]_c$ induced by high K^+, as well as their neuroprotective actions against free radicals or Ca^{2+} overload induced by high extracellular K^+ concentration.

To study a possible blockade of voltage-dependant Ca^{2+} channels (VDCC) by these compounds, which could prevent excess Ca^{2+} entry to the cells, SH-SY5Y human neuroblastoma cells, previously loaded with the fluorescent dye Fluo-4AM, were incubated in the presence of the compounds for 10 min and then stimulated with a concentrated solution of KCl, so that the final concentration was 70 mM K^+. Changes in fluorescence as a consequence of the $[Ca^{2+}]_c$ increase elicited by high K^+ concentrations were measured in a fluorescence plate-reader FluoStar Optima (BMG).

As shown in Table 4, the percentage of inhibition of $[Ca^{2+}]_c$ increase by compounds **1**–**5** was statistically significant. In fact, com-

Table 4
Effect of compounds **1**–**5** on the $[Ca^{2+}]_c$ increase elicited by 70 mM K^+ in SH-SY5Y cells (% inhibition with respect to a control without any drug)

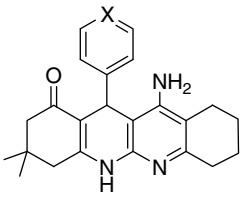

1-5

	X	% Inhibition in SH-SY5Y cells
Nimodipine[15b]	—	45.5 ± 6.1***
1	C-H	24.63 ± 3.55 ns
2	C-F	32.88 ± 3.65**
3	C-Me	30.95 ± 3.25**
4	C-OMe	31.04 ± 4.05**
5	N	45.11 ± 2.99***

All new compounds **1**–**5** and nimodipine were tested at the concentration of 0.3 μM.
Data are expressed as means ± SEM of at least three different cultures in quadruplicate; *$p < 0.05$; **$p < 0.01$; ***$p < 0.001$; ns, not significant.

pound **5** bearing the 4′-pyridyl ring gave a 45% blockade, which is higher than that found for the parent compound **1** and similar to that obtained for nimodipine.

2.4. Neuroprotection

The neuroprotective effect of compounds **1**–**5** was determined on SH-SY5Y cells exposed during 24 h to a medium with a depolarizing concentration of KCl (70 mM), which induces Ca^{2+} overload and the consequent cell death. Drugs, at the concentration of 0.3 μM, were administered 24 h before the incubation of cells with high K^+ (70 mM; hypertonic) and maintained for an additional 24 h. Thereafter, release of lactic dehydrogenase (LDH) into the medium was measured as a parameter of cell death.[27] Basal release of LDH by the cells was subtracted from the values obtained after incubation with 70 mM K^+ in the presence or absence of the compounds.

Compounds **1**–**5** proved to be strong neuroprotectants, with protection (%) values higher than those measured for tacrine or nimodipine (see Table 5). Interestingly, the neuroprotection was independent of the type of the substituent at the aromatic ring at C12, the best compound being molecule **3** (46%) with a 4′-Me group at C12.

Regarding neuroprotection against free radicals, compounds **1**–**5** were much less efficient than catalase, a neuroprotectant against free radical-induced toxicity, which was taken as a positive control. However, the compounds were more efficient than tacrine, which had any neuroprotecting effect (Table 6) and were slightly better than nimodipine. Compound **2**, which bears a 4′-F group at the aromatic ring, afforded the highest protection (around 47%).

To further determine if the protection against H_2O_2-induced toxicity could be due to a possible reactive oxygen species (ROS) scavenging effect of the compounds, we measured the reduction of fluorescence caused by the fluorescent dye H_2DCFDA in the presence of 60 μM H_2O_2 alone or in the presence of compounds **1**–**5**. None of the compounds tested decreased the fluorescence induced by H_2O_2 in a statistically significant manner (see Table 7).

3. Conclusions

The present study reports the synthesis and biological evaluation of tacripyrimedones, a series of new tacrine/1,4-dihydropyridine hybrids. Regarding AChE inhibition, compounds **1–5** have an inhibitory potency similar to that of tacrine, but are highly selective with respect to BuChE. These new compounds present a

Table 5
Cell viability in the presence of compounds **1**–**5** (0.3 μM), nimodipine (0.3 μM), and nimodipine (0.3 μM) expressed as % LDH released in the presence of 70 mM K^+ and % protection

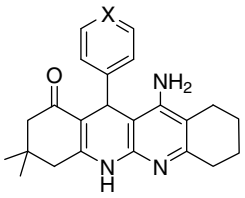

1-5

	X	LDH release (% vehicle)	% Protection
Tacrine[13]		90.4 ± 4.1 ns	13.4 ± 7.2
Nimodipine[13]		75.00 ± 2.24***	35.9 ± 2.8
1	C-H	68.9 ± 2.6***	40.7 ± 3.5
2	C-F	66.5 ± 2.5***	41.7 ± 2.9
3	C-Me	64.2 ± 0.0***	46.4 ± 1.5
4	C-OMe	65.5 ± 2.0***	44.1 ± 3.7
5	N	70.3 ± 2.3***	39.7 ± 2.7

Data are expressed as means ± SEM of at least three different cultures in quadruplicate. LDH released was calculated for each individual experiment considering 100% the extracellular LDH released in the presence of vehicle with respect to the total. To calculate % protection, LDH release was normalized as follows: In each individual quadruplicate experiment, LDH release obtained in non-treated cells (basal) was subtracted from the LDH released upon 70 K^+ treatment and normalized to 100% and that value was subtracted from 100 ***$p < 0.001$; ns, not significant.

Table 6
Cell viability in the presence of compounds **1**–**5** (0.3 μM), catalase (50 U/mL), tacrine (0.3 μM), and nimodipine (0.3 μM) expressed as % LDH released in the presence of 60 μM H_2O_2 and % protection

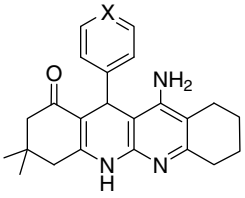

1-5

	X	LDH release (% vehicle)	% Protection
Catalase[13]	—	18.93 ± 1.77***	88.34 ± 2.80
Tacrine[13]	—	100.34 ± 3.37 ns	0
Nimodipine[13]	—	75.42 ± 2.12***	36.03 ± 2.82
1	C-H	86.44 ± 3.69**	17.40 ± 4.85
2	C-F	64.39 ± 1.24***	46.84 ± 1.53
3	C-Me	84.35 ± 3.39***	20.17 ± 4.48
4	C-OMe	69.02 ± 2.72***	40.73 ± 3.49
5	N	69.94 ± 2.08***	39.66 ± 2.80

Data are expressed as means ± SEM of at least three different cultures in quadruplicate. LDH released was calculated for each individual experiment considering 100% the extracellular LDH released in the presence of vehicle with respect to the total. To calculate % protection, LDH release was normalized as follows: In each individual quadruplicate experiment, LDH release obtained in non-treated cells (basal) was subtracted from the LDH released upon 60 μM H_2O_2 treatment and normalized to 100% and that value was subtracted from 100. **$p < 0.01$; ***$p < 0.001$; ns, not significant.

Table 7
Decrease of H_2O_2-generated reactive oxygen species (ROS) in the presence of compounds **1–5** (0.3 μM) and catalase (50 U/mL) expressed as % fluorescence induced by 60 μM H_2O_2

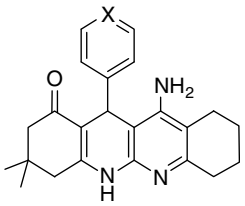

1-5

	X	Fluorescence (% H_2O_2)
Vehicle	—	100
Catalase	—	$31 \pm 6.2^{***}$
1	C-H	87.9 ± 7.7^{ns}
2	C-F	95.7 ± 5.6^{ns}
3	C-Me	79.9 ± 8.1^{ns}
4	C-OMe	87.8 ± 3.2^{ns}
5	N	82.9 ± 3.1^{ns}

Data are expressed as means ± SEM of at least three different experiments in quadruplicate. $^{***}p < 0.001$; ns, not significant.

non-competitive type of AChE inhibition, suggesting that they bind to the PAS of the enzyme, as confirmed by the results of docking studies, which indicates that the inhibitory potency should be mainly ascribed to the *R*-enantiomer. Moreover, the predicted binding mode also allows us to explain the nearly 100-fold increase in potency arising upon replacement of the oxygen atom at C4 in **19**–**22** by the naphthyridine NH unit present in **1-5**. K_i values show that tacripyrimedones present a high nanomolar affinity for the PAS center of the enzyme.

Compounds **1–5** decreased the rise in $[Ca^{2+}]_c$ induced by K^+ in neuroblastoma cells. This effect correlates with their neuroprotective effect against Ca^{2+} overload, which was significant for all compounds and independent of the type of substituent. Finally, products **1–5** were also neuroprotective against free radical toxicity with values of protection ranging from 17% to 40%, at the concentration of 0.5 μM, the most active being compound **2**, which bears a 4′-F group. This effect was not probably due to scavenging of ROS, since none of the compounds reduced in a significant manner the fluorescence due to H_2O_2, measured with the fluorescent dye H_2DCFDA.

Based on these findings, tacripyrimedones **1–5** appear to be promising compounds, and the present molecular modeling results provide a relevant basis to pursue our efforts by exploring the structure–activity relationships of enantiomerically pure *R*- and *S*-tacripyrimedones.

4. Experimental

4.1. General methods

Reactions were monitored by TLC using precoated silica gel aluminum plates containing a fluorescent indicator (Merck, 5539). Detection was done by UV (254 nm) followed by charring with sulfuric–acetic acid spray, 1% aqueous potassium permanganate solution, or 0.5% phosphomolybdic acid in 95% EtOH. Anhydrous Na_2SO_4 was used to dry organic solutions during work-ups and the removal of solvents was carried out under vacuum with a rotary evaporator. Flash column chromatography was performed using silica gel 60 (230–400 mesh, Merck). Melting points were determined on a Kofler block and are uncorrected. IR spectra were obtained on a Perkin-Elmer Spectrum One spectrophotometer. ^{1}H NMR spectra were recorded with a Varian VXR-200S spectrometer, using tetramethylsilane as internal standard and ^{13}C NMR spectra were recorded with a Bruker WP-200-SY. All the assignments for protons and carbons were in agreement with 2D COSY, gHSQC, gHMBC, and 1D NOESY spectra. Elemental analyses were carried out on a Carlo Erba EA 1108 apparatus.

4.2. General method for the Friedländer reaction

Aluminum chloride (1.2–1.7 equiv) was suspended in dry 1,2-dichloroethane (10 mL) at rt under argon. The corresponding dihydropyridine (1 equiv) and cyclohexanone (1.2–1.7 equiv) were added. The reaction mixture was heated under reflux (10–24 h). When the reaction was over (TLC analysis), a mixture of THF/H_2O (1:1) was added at rt. An aqueous solution of sodium hydroxide (10%) was added dropwise to the mixture until the aqueous solution was basic. After stirring for 30 min, the mixture was extracted three times with dichloromethane. The organic layer was washed with brine, dried over anhydrous sodium sulfate, filtered, and the solvent was evaporated. The resultant solid was purified by silica gel flash chromatography using methanol/dichloromethane mixtures as eluent to give pure compounds.

4.2.1. 11-Amino-3,3-dimethyl-3,4,5,7,8,9,10,12-octahydro-12-phenyl-dibenzo[*b*,*g*][1,8] naphthyridine-1(2*H*)-one (1)

Following the procedures Section 4.1, the reaction of compound 6[15a] (200 mg, 0.68 mmol) with $AlCl_3$ (136 mg, 1.02 mmol), in $ClCH_2CH_2Cl$ (5 mL), and cyclohexanone (100 mg, 1.02 mmol), after 3 h, gave product 1 (247 mg, 97%): mp 325–327 °C; IR (KBr) *ν* 3393, 3225, 2931, 2862, 1616, 1600, 1439, 1396, 1246 cm^{-1}; ^{1}H NMR (see Table 8); ^{13}C NMR (see Table 9); MS (API-ES$^+$) *m*/*z*: $[M+1]^+$ 374.2; $[M+Na]^+$ 396.1; $[M+K]^+$ 412.2; $[2M+Na]^+$ 769.5. Anal. Calcd for $C_{24}H_{27}N_3O$: C, 77.18; H, 7.29; N, 11.25. Found: C, 76.99; H, 7.30; N, 11.14.

4.2.2. 11-Amino-12-(4′-fluorophenyl)-3,3-dimethyl-3,4,5,7,8,9,10,12-octahydrodibenzo [*b*,*g*][1,8]naphthyridine-1(2*H*)-one (2)

Following the procedures in Section 4 and 1, the reaction of compound **7**[15a] (200 mg, 0.64 mmol) with $AlCl_3$ (128 mg, 0.96 mmol) and cyclohexanone (94 mg, 0.96 mmol), in $ClCH_2CH_2Cl$ (5 mL), after 4.5 h, gave molecule **2** (300 mg, 90%): mp 325–327 °C; IR (KBr) *ν* 3396, 3217, 2931, 2862, 1616, 1504, 1441, 1396, 1245 cm^{-1}; ^{1}H NMR (see Table 8); ^{13}C NMR (see Table 9); MS (API-ES$^+$) *m*/*z*: $[M+1]^+$ 392.3; $[M+Na]^+$ 415.2; $[2M+Na]^+$ 807.3. Anal. Calcd for $C_{24}H_{26}FN_3O$: C, 73.63; H, 6.69; N, 10.73. Found: C, 73.48; H, 6.57; N, 10.48.

4.2.3. 11-Amino-3,3-dimethyl-12-(4′-methylphenyl)-3,4,5,7,8,9,10,12-octahydrodibenzo[*b*,*g*][1,8]naphthyridine-1(2*H*)-one (3)

Following the procedures in Section 4.1, the reaction of compound 8[15a] (200 mg, 0.65 mmol) with $AlCl_3$ (146 mg, 0.97 mmol) and cyclohexanone (96 mg, 0.97 mmol), in $ClCH_2CH_2Cl$ (5 mL), after 4 h, afforded compound 3 (243 mg, 96%): mp 336–338 °C; IR (KBr) *ν* 3394, 3217, 29.31, 2862, 1614, 1600, 1439, 1246 cm^{-1}; ^{1}H NMR (see Table 8); ^{13}C NMR (see Table 9); MS (API-ES$^+$) *m*/*z*: $[M+1]^+$ 388.3; $[M+Na]^+$ 410.2; $[2M+Na]^+$ 797.5. Anal. Calcd for $C_{25}H_{29}N_3O$: C, 77.48; H, 7.54; N, 10.84. Found: C, 77.35; H, 7.66; N, 10.57.

4.2.4. 11-Amino-12-(4′-methoxyphenyl)-3,3-dimethyl-3,4,5,7,8,9,10,12-octahidrodibenzo[*b*,*g*][1,8]naphthyridine-1(2*H*)-one (4)

Following procedures in Section 4.1, the reaction of compound 9[15a] (200 mg, 0.61 mmol) with $AlCl_3$ (123 mg, 0.92 mmol) and cyclohexanone (91 mg, 0.92 mmol), in $ClCH_2CH_2Cl$ (5 mL), after 5 h, provided product 4 (203 mg, 83%): mp 318–320 °C; IR (KBr)

Table 8
Selected ^{1}H NMR (DMSO-d_6, 300 MHz, δ) for compounds **1–5**

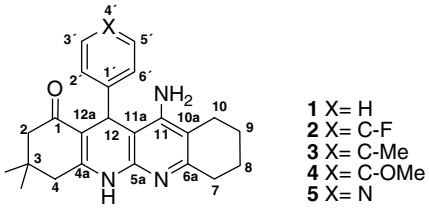

1 X= H
2 X= C-F
3 X= C-Me
4 X= C-OMe
5 X= N

(**1-5**)

	NH	NH_2	H12	H_2	H4	H7	H10	H9,H8	$(CH3)_2C3$
1	9.54 (s)	5,40 (s)	5.12 (s)	2.52–2.36 J_{AB} = 16.1	2.23–1.96 J_{AB} = 16.0	2.61 (s)	2.34–2.20 (m)	1.73 (s)	1.04, 0.87 (s)
2	9.50 (s)	5.36 (s)	5.09 (s)	2.44–2.27 J_{AB} = 17.0	2.15–1.87 J_{AB} = 16.0	2.53 (s)	2.30–1.92 (m)	1.66 (s)	0.97, 0.80 (s)
3	9.44 (s)	5.25 (s)	4.99 (s)	2.49–2.34 J_{AB} = 16.0	2.14–1.88 J_{AB} = 16.0	2.52 (s)	2.33–2.13 (m)	1.65 (s)	0.97, 0.87 (s)
4	9.42 (s)	5.25 (s)	4.98 (s)	2.48–2.27 J_{AB} = 17.0	2.14–1.89 J_{AB} = 16.0	2.53 (s)	2.29–2.18 (m)	1.66 (s)	0.97, 0.82 (s)
5	9.59 (s)	5.47 (s)	5.15 (s)	2.6–2.8 J_{AB} = 17.	2.16–1.91 J_{AB} = 16.0	2.53 (s)	2.20–2.18 (m)	1.66 (s)	0.97, 0.82 (s)

Table 9
Selected ^{13}C NMR (DMSO-d_6, 300 MHz, δ) for compounds **1–5**

	C2	C3	C4	C4a	C5a	C6a	C7	C8	C9	C10	C10a	C11	C11a	C12	C12a
1	50.6	32.4	40.1	152.2	152.4	147.1	32.2	22.6	22.7	23.2	111.5	150.4	100.8	34.9	107.9
2	50.5	32.4	40.1	152.8	150.4	147.1	32.2	22.6	22.7	23.2	111.5	150.3	100.5	34.1	107.8
3	50.6	32.4	40.1	152.3	152.2	147.1	32.2	22.6	22.8	23.2	111.5	150.3	100.9	34.6	108.0
4	50.2	32.6	40.3	151.8	151.7	146.7	31.8	22.3	22.4	22.9	111.1	150.9	100.7	33.7	107.8
5	50.4	32.4	40.1	153.2	152.8	147.2	32.2	22.6	22.7	23.2	111.6	150.6	99.1	34.4	106.5

v 3390, 3210, 2934, 1609, 1601, 1507, 1439, 1249 cm^{-1}; ^{1}H NMR (see Table 8); ^{13}C NMR (see Table 9); MS (API-ES$^+$) *m*/*z*: [M+1]$^+$ 404.2; [M+Na]$^+$ 426.2; [2M+Na]$^+$ 829.0. Anal. Calcd for $C_{25}H_{29}N_3O_2$: C, 74.41; H, 7.24; N, 10.41. Found: C, 74.33; H, 7.15; N, 10.37.

4.2.5. 11-Amino-3,3-dimethyl-3,4,5,7,8,9,10,12-octahydro-12-(4′-pyridyl)-dibenzo[*b*,*g*][1,8]naphthyridine-1(*2H*)-one (5)

Following the procedures in Section 4.1, the reaction of compound 10[15b] (200 mg, 0.68 mmol) with $AlCl_3$ (136 mg, 1.02 mmol) and cyclohexanone (100 mg, 1.02 mmol), in $ClCH_2CH_2Cl$ (5 mL), after 4 h, furnished compound 10 (221 mg, 88%): mp 315–318 °C; IR (KBr) *v* 3392, 3227, 2932, 2869, 1618, 1601, 1499, 1441, 1245 cm^{-1}; ^{1}H NMR (see Table 8); ^{13}C NMR (see Table 9); MS (API-ES$^+$) *m*/*z*: [M+1]$^+$ 375.2; [M+Na]$^+$ 397.2; [2M+Na]$^+$ 771.5. Anal. Calcd for $C_{23}H_{26}N_4O$: C, 73.77; H, 7.00; N, 14.96. Found: C, 74.02; H, 6.98; N, 14.87.

4.3. Pharmacological studies

4.3.1. Measurement of AChE activity in *Electrophorus electricus*

To assess the inhibitory activity of the compounds toward AChE, we followed the spectrophotometric method of Rappaport[17] using purified AChE from Electric eel (*E. electricus*) and acetylcholine chloride (29.5 mM) as a substrate. The reaction took place in a final volume of 2.5 mL of an aqueous solution containing 0.78 U AChE and 1.9 mM *m*-nitrophenol to produce a yellow color which is lost as a function of enzyme activity. Inhibition curves were made by incubating with the different compounds for 30 min; a sample without any compound was always present to determine the 100% of enzyme activity. After the 30 min incubation, the loss of yellow color by *m*-nitrophenol was evaluated by measuring absorbance at 405 nm in a spectrophometric plate reader (iEMS Reader MF, Labsystems). The concentration of compound that produces 50% AChE activity inhibition (IC_{50}) was calculated by transforming the values of absorbance to Rappaport enzymatic activity units extrapolating from a calibration curve previously obtained. Data are means ± SEM of at least three different experiments in triplicate.

4.3.2. Measurement of AChE activity in hAChE

The inhibitory activity of the compounds toward hAChE was determined following the method of Ellman[18] using AChE from human erythrocytes and acetylthiocholine chloride (0.53 mM) as a substrate. The reaction took place in a final volume of 3 mL of a phosphate-buffered solution at pH 8, containing 0.09 U of hAChE and 333 μM of 5,5′-dithiobis-2-nitrobenzoic acid (DTNB), which produces the yellow anion 5-thio-2-nitrobenzoic acid. Inhibition curves were made by incubating with the different compounds for 15 min; a sample without any compound was always present to determine the 100% of enzymatic activity. After the 15 min incubation period, the production of color, as an indication of enzymatic activity, was evaluated by measuring absorbance at 412 nm in a spectrophotometer plate reader (iEMS Reader MF, Labsystems).

4.3.3. Measurement of BuChE activity

The inhibitory activity of the compounds toward BuChE was determined following the method of Ellman[18] using BuChE from human serum and butyrylthiocholine chloride (5 mM) as a substrate. The reaction took place in a final volume of 1 mL of a phosphate-buffered solution at pH 7.2, containing 0.035 U of BuChE and 0.25 mM 5,5′-dithiobis-2-nitrobenzoic acid (DTNB), which produces the yellow anion 5-thio-2-nitrobenzoic acid. Inhibition curves were made by incubating with the different compounds for 15 min; a sample without any compound was always present to determine the 100% of enzymatic activity. After the 15 min incubation period, the production of color, as an indication of enzymatic activity, was evaluated by measuring absorbance at 412 nm in a spectrophotometric plate reader (iEMS Reader MF, Labsystems).

4.3.4. Kinetic characterization of AChE inhibition

Acetylcholinesterase (*Electric eel*), DTNB, and acetylthiocholine were purchased from Sigma–Aldrich chemical company. Inhibitors were solubilized in DMSO at a stock concentration of 10^{-2} M and maintained at +4 °C. AChE inhibition was assayed spectrophotometrically at 30 °C according to the method of Ellman.[18] Assay buffer was phosphate-buffered solution (PBS) 0.1 M, pH 8.0. A stock solution of AChE (270 U/mL) in assay buffer was kept at −80 °C, and a 1:70 dilution was prepared immediately before starting the measurement. ATCh (10 mM) and DTNB (1 mM) were dissolved in assay buffer and kept at −80 °C. Tacrine–HCl was dissolved in water and stock solutions of compounds **1–5** were prepared in DMSO. For inhibitors, at least five concentrations were used.

Experiments were performed in a transparent 48-well plate containing each well 350 μL of the DTNB solution, variable volumes of buffer solution between 604 and 504 μL, 1 μL DMSO or inhibitor solution to give desired final concentration, and five different concentrations of ATCh (0.1, 0.25, 0.5, 0.75, and 1 mM). The mixture was thoroughly mixed. The reaction was initiated by adding 45 μL of an AChE solution (0.18 U/mL) at 30 °C to give a final volume of 1 mL. Uninhibited enzyme activity was determined by adding DMSO instead of the inhibitor solution. Determination of Michaelis constant for the substrate ATCh was done at 6 different concentrations (0.1–1.5 mM) to give a value of $K_m = 650 \pm 40$ μM, and $V_{max} = 1.48 \pm 0.05$ min^{-1}. The rates of AChE-catalyzed ATCh hydrolysis were corrected by those of the non-enzymatic hydrolysis of ATCh as determined by using 45 μL of assay buffer, instead of the enzyme solution. Progress curves were monitored at 412 nm over 2 min in a fluorescence plate-reader Fluostar Optima (BMG-technologies, Germany) absorbance ready. Progress curves were characterized by a linear steady-state turnover of the substrate and values of a linear regression were fitted according to Lineweaver–Burk replots using Origin software (version 7.0). Double reciprocal plots were generated using the same statistical package. The relative K_i's and types of inhibition were determined by plotting the slopes of the double reciprocal plots versus concentration of inhibitor as described elsewhere.[28] Briefly, from the initial Michaelis–Menten equation for Lineweaver–Burk plot that one for a mixed non-competitive inhibition is developed

$$(1/V_0 = 1/V_{max} + (K_M/V_{max})/[S]) \quad (1)$$

$$\frac{1}{V_o} = \left(1 + \frac{[I]}{K_I}\right)\frac{1}{V_{max}} + \frac{K_M}{V_{max}}\left(1 + \frac{[I]}{K_i}\right)\frac{1}{[S]}, \quad (2)$$

where the slope for each inhibitor concentration is

$$\rho = (K_M/V_{max})(1 + [I]/K_i) \quad (3)$$

or written as a "$y = a + bx$" equation

$$\rho = \frac{K_M}{V_{max}} + \frac{K_M}{V_{max} \cdot K_i}[I] \quad (4)$$

Thus, representing slopes *versus* concentration inhibitor, we can calculate K_M/V_{max} from y axis intercept (parameter a) and the K_i as a/b. All rate measurements were performed in quadruplicate.

4.3.5. Culture of SH-SY5Y cells

SH-SY5Y cells, at passages between 3 and 16 after de-freezing, were maintained in a Dulbecco's modified Eagle's medium (DMEM) containing 15 non-essential amino-acids (NEAAs) and supplemented with 10% fetal calf serum (FCS), 1 mM glutamine, 50 U/mL penicillin, and 50 μg/mL streptomycin (reagents from GIBCO, Madrid, Spain). Cultures were seeded into flasks containing supplemented medium and maintained at 37 °C in 5% CO_2/humidified air. Stock cultures were passaged 1:4 twice weekly. For assays, SH-SY5Y cells were sub-cultured in 48-well plates at a seeding density of 2×10^5 cells per well, or in 96-well plates at a seeding density of 8×10^4 cells per well. For the cytotoxicity experiments, cells were treated with drugs before confluence, in DMEM free of serum.

4.3.6. Measurement of cytosolic Ca^{2+} concentrations

For these experiments, SH-SY5Y neuroblastoma cells were grown at confluence in 96-well black dishes. Cells were loaded with 4 μM fluo 4/AM for 1 h at 37 °C in DMEM. Then, cells were washed twice with Krebs–Hepes solution and kept at room temperature for 30 min before the beginning of the experiment. Fluorescence was measured in a fluorescence microplate reader (FLUOstar Optima, BMG, Germany). Wavelengths of excitation and emission were 485 and 520 nm, respectively.

4.3.7. Measurement of lactic dehydrogenase (LDH) activity

Extracellular and intracellular LDH activity was spectrophotometrically measured using a Cytotoxicity Cell Death kit (Roche-Boehringer. Mannheim, Germany) according to the manufacturer's indications. Total LDH activity was defined as the sum of intracellular and extracellular LDH activity; released LDH was defined as the percentage of extracellular compared to total LDH activity.

4.3.8. Measurement of reactive oxygen species (ROS)

To measure cellular ROS, we have used the molecular probe H_2DCFDA.[29] SH-SY5Y cells were loaded with 10 μM/L H_2DCFDA, which diffuses through the cell membrane and is hydrolyzed by intracellular esterases to the non-fluorescent form dichlorofluorescein (DCFH). DCFH reacts with intracellular H_2O_2 to form dichlorofluorescein (DFC), a green fluorescent dye. Fluorescence was measured in a fluorescence microplate reader (FLUOstar Optima, Biogen). Wavelengths of excitation and emission were 485 and 520 nm, respectively.

4.3.9. Molecular modeling

Docking was performed with the program rDock, which is an extension of the program RiboDock[30] using an empirical scoring function calibrated based on protein–ligand complexes.[31] This program uses an empirical scoring function for attractive and repulsive polar interactions in combination with a Lennard–Jones potential to account for the van der Waals term. Ligand internal energies are accounted for using the same terms as the intermolecular potential, plus a dihedral potential derived from the Tripos force field.[32] A full search can be performed using a genetic algorithm where ligand docking poses are represented using a conventional chromosome representation of translation, rotation, and rotatable bond dihedral angles, while the receptor site was kept fixed.

The reliability of rDock was assessed by docking tacrine at the catalytic site of the *Torpedo californica* AChE and propidium at the peripheral site of the mouse AChE, taking advantage of the X-ray crystallographic structures of the two complexes (PDB entries 1ACJ and 1N5R).[33,34] Docking of compound **4** was performed using a structural model of the human enzyme used in our previous studies.[35,36] Superposition of the X-ray crystallographic structures confirmed unambiguously the structural similarity of the ligand-binding sites. Water molecules were removed from the coordinates, and the docking volume was defined as the space within 10 Å of the ligands for both catalytic and peripheral binding sites. Before docking, the structure of the ligands was built up and energy minimized at the MP2/6-31G* level using Gaussian03.[37] Each compound was subjected to 100 docking runs, and the output docking modes were analyzed by visual inspection in conjunction with the docking scores.

Acknowledgments

R.L. thanks the Ministerio de Educación y Ciencia (MEC) for a fellowship (AP20020576). This work was supported by Fundación Teófilo Hernando, FMUAM Red CIEN (Instituto de Salud Carlos III), MEC (Grants Nos. BFI2003-02722; SAF2006-08764-C02-01; SAF2006-08540; CTQ2005-08797), Instituto de Salud Carlos III [Retic "RENEVAS" (RD06-2006-1002)], Comunidad de Madrid S/SAL-0275-2006), CSIC-GRICES project (2007PT-13), AECI (A/7492/07).

References

1. Scarpini, E.; Scheltens, P.; Feldman, H. *Lancet Neurol.* **2003**, *2*, 539.
2. Talesa, V. N. *Mech. Ageing Dev.* **2001**, *122*, 1961.
3. Lahiri, D. K.; Rogers, J. T.; Greig, N. H.; Sambamurti, K. *Curr. Pharm. Des.* **2004**, *10*, 3111.
4. Selkoe, D. J. *Annu. Rev. Neurosci.* **1989**, *12*, 463.
5. (a) Kruman, I.; Guo, Q.; Mattson, M. P. *J. Neurosci. Res.* **1998**, *51*, 293; (b) Mattson, M. P.; Cheng, B.; Davis, D.; Bryant, K.; Lieberburg, I.; Rydel, R. F. *J. Neurosci.* **1992**, *12*, 376.
6. Cano-Abad, M. F.; Villarroya, M.; García, A. G.; Gabilán, N. H.; López, M. G. *J. Biol. Chem.* **2001**, *276*, 39695.
7. (a) Espinoza-Fonseca, L. M. *Bioorg. Med. Chem.* **2006**, *14*, 896; (b) Youdim, M. B. H.; Buccafusco, J. *J. Trends Pharmacol. Sci.* **2005**, *26*, 27; (c) Morphy, R.; Rankovic, Z. *J. Med. Chem.* **2005**, *48*, 6523; (d) Meunier, B. *Acc. Chem. Res.* **2008**, *41*, 69; (e) Decker, M. *J. Med. Chem.* **2006**, *49*, 5411; (f) Muñoz-Ruiz, P.; Rubio, L.; García-Palomero, E.; Dorronsoro, I.; del Monte-Millán, M.; Valenzuela, R.; Usán, P.; de Austria, C.; Bartolini, M.; Andrisano, V.; Bidon-Chanal, A.; Orozco, M.; Luque, F. J.; Medina, M.; Martínez, A. *J. Med. Chem.* **2005**, *48*, 7223.
8. (a) Rodríguez-Franco, M. I.; Fernández-Bachiller, M. I.; Pérez, C.; Hernández-Ledesma, B.; Bartolomé, B. *J. Med. Chem.* **2006**, *49*, 459; (b) Sterling, J.; Herzig, Y.; Goren, T.; Finkelstein, N.; Lerner, D.; Goldenberg, W.; Miskolczi, I.; Molnar, S.; Rantal, F.; Tamas, T.; Toth, G.; Zagyva, A.; Zekany, A.; Lavian, G.; Gross, A.; Friedman, R.; Razin, M.; Huang, W.; Krais, B.; Chorev, M.; Youdim, M. B.; Weinstock, M. *J. Med. Chem.* **2002**, *45*, 5260; (c) Toda, N.; Tago, K.; Marumoto, S.; Takami, K.; Ori, M.; Yamada, N.; Koyama, K.; Naruto, S.; Abe, K.; Yamazaki, R.; Hara, T.; Aoyagi, A.; Abe, Y.; Kaneko, T.; Kogen, H. *Bioorg. Med. Chem.* **2003**, *11*, 4389; (d) Bolognesi, M. L.; Banzi, R.; Bartolini, M.; Cavalli, A.; Tarozzi, A.; Andrisano, V.; Minarini, A.; Rosini, M.; Tumiatti, V.; Bergamini, C.; Fato, R.; Lenaz, G.; Hrelia, P.; Cattaneo, A.; Recanatini, M.; Melchiorre, C. *J. Med. Chem.* **2007**, *59*, 4882; (e) Elsinghorst, P. W.; Cieslik, J. S.; Mohr, K.; Tränkle, C.; Gütschow, M. *J. Med. Chem.* **2007**, *50*, 5685.
9. Choudhary, M. I.; Nawaz, S. A.; Haq, Z.; Azim, M. K.; Ghayur, M. N.; Lodhi, M. A.; Jalil, S.; Khalid, A.; Ahmed, A.; Rode, B. M.; Rahman, A.; Gilani, A. H.; Ahmad, V. U. *Biochem. Biophys. Res. Commun.* **2005**, *332*, 1171.
10. Perry, G.; Cash, A. D.; Smith, M. A. *J. Biomed. Biotechnol.* **2002**, *2*, 120.
11. Tan, D. X.; Manchester, L. C.; Sainz, R.; Mayo, J. C.; Alvares, F. L., et al *Expert Opin. Ther. Pat.* **2003**, *13*, 1513.
12. Klatte, E. T.; Scharre, D. W.; Nagaraja, H. N.; Davis, R. A.; Beversdorf, D. Q. *Alzheimer Dis. Assoc. Disord.* **2003**, *17*, 113.
13. Marco-Contelles, J.; León, R.; de los Ríos, C.; Guglietta, A.; Terencio, J.; López, M. G.; García, A. G.; Villarroya, M. *J. Med. Chem.* **2006**, *49*, 7607.
14. Cheng, C. C.; Yan, S. *J. Org. React.* **1982**, *28*, 37.
15. For compounds **6**–**9**, see (a) Tu, S.; Zhang, J.; Zhu, X.; Zhang, Y.; Wang, Q.; Xu, J.; Jiang, B.; Jia, R.; Zhang, J.; Shi, F. *J. Heterocycl. Chem.* **2006**, *43*, 985. and references cited therein; Compound **10** has been reported in (b) León, R.; de los Ríos, C.; Marco-Contelles, J.; López, M. G.; García, A. G.; Villarroya, M. *Eur. J. Med. Chem.* **2008**, *43*, 668; (c) Marco-Contelles, J.; León, R.; de los Ríos, C.; García, A. G.; López, M. G.; Villarroya, M. *Bioorg. Med. Chem.* **2006**, *14*, 8176.
16. León, R.; Marco-Contelles, J.; García, A. G.; Villarroya, M. *Bioorg. Med. Chem.* **2005**, *13*, 1167. and references cited therein.
17. Rappaport, F.; Fischl, J.; Pinto, N. *Clin. Chim. Acta* **1959**, *4*, 227.
18. Ellman, G. L.; Courtney, K. D.; Andres, B., Jr.; Featherstone, R. M. *Biochem. Pharmacol.* **1961**, *7*, 88.
19. (a) Marco, J. L.; de los Ríos, C.; García, A. G.; Villarroya, M.; Carreiras, M. C.; Martins, C.; Eléuterio, A.; Morreale, A.; Orozco, M.; Luque, F. *J. Bioorg. Med. Chem.* **2004**, *12*, 2199; (b) Marco, J. L.; de los Ríos, C.; Carreiras, M. C.; Baños, J. E.; Badía, A.; Vivas, N. M. *Bioorg. Med. Chem.* **2001**, *9*, 727.
20. Marco-Contelles, J.; León, R.; López, M. G.; García, A. G.; Villarroya, M. *Eur. J. Med. Chem.* **2006**, *41*, 1464.
21. (a) Chatonnet, A.; Lockridge, O. *Biochem. J.* **1989**, *260*, 625–634; (b) Bartolini, M.; Bertucci, C.; Cavrini, V.; Andrisano, V. *Biochem. Pharmacol.* **2003**, *65*, 407.
22. (a) Álvarez, A.; Alarcón, R.; Opazo, C.; Campos, E. O.; Muñoz, F. J.; Calderón, F. H.; Dajas, F.; Gentry, M. K.; Doctor, B. P.; De Mello, F. G.; Inestrosa, N. C. *J. Neurosci.* **1998**, *18*, 3213; (b) Campos, E. O.; Álvarez, A.; Inestrosa, N. C. *Neurochem. Res.* **1998**, *23*, 135.
23. (a) Inestrosa, N . C.; Álvarez, A.; Pérez, C. A.; Moreno, R. D.; Vicente, M.; Linker, C.; Casanueva, O. I.; Soto, C.; Garrido, J. *Neuron* **1996**, *16*, 881; (b) Inestrosa, N. C.; Álvarez, A.; Calderón, F. *Mol. Psychiatry* **1996**, *1*, 359.
24. Radic, Z.; Reiner, E.; Taylor, P. *Mol. Pharmacol.* **1991**, *39*, 98.
25. Krupka, R. M.; Laidler, K. J. *J. Am. Chem. Soc.* **1961**, *83*, 1454.
26. Rampa, A.; Bisi, A.; Belluti, F.; Gobbi, S.; Valenti, P.; Andrisano, V.; Cavrini, V.; Cavalli, A.; Recanatini, M. *Bioorg. Med. Chem.* **2000**, *8*, 497.
27. Maroto, R.; De la Fuente, M. T.; Artalejo, A. R.; Abad, F.; López, M. G.; García-Sancho, J.; García, A. G. *Eur. J. Pharmacol.* **1994**, *270*, 331.
28. *Enzyme Kinetics*; Segel, I. H., Ed.; John Wiley: Toronto, 1975.
29. Ha, H. C.; Woster, P. M.; Yager, J. D.; Casero, R. A. *Proc. Natl. Acad. Sci. U.S.A.* **1997**, *94*, 11557.
30. Morley, S. D.; Afshar, M. *J. Comput.-Aided Mol. Des.* **2004**, *18*, 189.
31. Barril, X.; Hubbard, R. E.; Morley, S. D. *Mini-Rev. Med. Chem.* **2004**, *4*, 779.
32. Clark, M.; Cramer, R. D., III; Van Opdenbosch, N. *J. Comput. Chem.* **1989**, *10*, 982.
33. Harel, M.; Schalk, I.; Ehret-Sabatier, L.; Bouet, F.; Goeldner, M.; Hirth, C.; Axelsen, P. H.; Silman, I.; Sussman, J. L. *Proc. Natl. Acad. Sci. U.S.A.* **1993**, *90*, 9031.
34. Bourne, Y.; Taylor, P.; Radic, Z.; Marchot, P. *EMBO J.* **2003**, *22*, 1.
35. Camps, P.; Formosa, X.; Galdeano, C.; Gómez, T.; Muñoz-Torrero, D.; Scarpellini, M.; Viayna, E.; Badia, A.; Clos, M. V.; Camins, A.; Pallàs, M.; Bartolini, M.; Mancini, F.; Andriasno, V.; Estelrich, J.; Lizondo, M.; Bidon-Chanal, A.; Luque, F. J. *J. Med. Chem.* **2008**, *51*, 3588.
36. Kryger, G.; Harel, M.; Giles, K.; Toker, L.; Velan, B.; Lazar, A.; Kronman, C.; Barak, D.; Ariel, N.; Shafferman, A.; Silman, I.; Sussman, J. L. *Acta Crystallogr. Sect. D* **2000**, *56*, 1385.
37. Frisch, M. J.; Trucks, G. W.; Schlegel, H. B.; Scuseria, G. E.; Robb, M. A.; Cheeseman, J. R.; Montgomery, J. A., Jr.; Vreven, T.; Kudin, K. N.; Burant, J. C.; Millam, J. M.; Iyengar, S. S.; Tomasi, J.; Barone, V.; Mennucci, B.; Cossi, M.; Scalmani, G.; Rega, N.; Petersson, G. A.; Nakatsuji, H.; Hada, M.; Ehara, M.; Toyota, K.; Fukuda, R.; Hasegawa, J.; Ishida, M.; Nakajima, T.; Honda, Y.; Kitao, O.; Nakai, H.; Klene, M.; Li, X.; Knox, J. E.; Hratchian, H. P.; Cross, J. B.; Adamo, C.; Jaramillo, J.; Gomperts, R.; Stratmann, R. E.; Yazyev, O.; Austin, A. J.; Cammi, R.; Pomelli, C.; Ochterski, J. W.; Ayala, P. Y.; Morokuma, K.; Voth, G. A.; Salvador, P.; Dannenberg, J. J.; Zakrzewski, V. G.; Dapprich, S.; Daniels, A. D.; Strain, M. C.; Farkas, O.; Malick, D. K.; Rabuck, A. D.; Raghavachari, K.; D. K. Malick, Foresman, J. B.; Ortiz, J. V.; Cui, Q.; Baboul, A. G.; Clifford, S.; Cioslowski, J.; Stefanov, B. B.; Liu, G.; Liashenko, A.; Piskorz, P.; Komaromi, I.; Martin, R. L.; Fox, D. J.; Keith, T.; Al-Laham, M. A.; Peng, C. Y.; Nanayakkara, A.; Challacombe, M.; Gill, P. M. W.; Johnson, B.; Chen, W.; Wong, M. W.; González, C.; Pople, J. A. Gaussian 03, Revision B.04, Gaussian, Inc., Pittsburgh PA, 2003.